Study of the Transition Effect with the ATLAS Tile calorimeter

J.A.Budagov [1], **A.M.Henriques** [2], **G.D.Khoriauli** [1, 3], **J.I.Khubua** [1, 4], **Y.A.Kulchitsky** [1, 5], **N.A.Rusakovich** [1], **P.V.Tsiareshka** [1, 5], **V.B.Vinogradov** [1]

[1] JINR, Dubna, Russia
[2] CERN, Geneva, Switzerland
[3] TSU Tbilisi, Georgia
[4] TSU HEPI Tbilisi, Georgia
[5] IP National Academy of Sciences, Minsk, Belarus

Abstract

With the aim of establishing the electromagnetic response energy scale of the ATLAS Tile calorimeter and understanding the performance of the calorimeter to electrons 12 % of the modules have been exposed to electron beams with various energies. On the basis of the obtained electromagnetic calibration constants we have determined the *e/mip* values in function of the absorber thickness using different beam incident angles. We have observed the transition effect ($e/mip < 1$) and, for the first time, its behaviour as a function of the absorber thickness — the *e/mip* ratio decreases logarithmically when the absorber thickness increases and this is well described by the GEANT4 (version 6.2) Monte-Carlo simulation. These results are important for precision electromagnetic energy scale determination for the ATLAS Tile calorimeter.

1 Introduction

The ATLAS detector at the LHC has a huge physics discovery potential, in particular in the detection of a heavy Higgs boson [1, 2]. Calorimeters will play a crucial role in it. The key question of calorimetry is the absolute energy calibration,in particular the calibration in the electromagnetic energy scale.

The electromagnetic energy scale is of great interest due to a very fundamental property of calorimeters which is the signal linearity for electromagnetic showers.

With the aim of establishing of this scale and understanding of performance of the ATLAS Tile hadronic calorimeter (TileCal) [3] to electrons 12 % of modules have been exposed to electron beams with various energies (from 10 GeV to 180 GeV) in three different geometries: the beam enters in the center of each A cell with an incident angle of 20^o, η-scan and tilerow scan at $\theta = 90^o$ for the module side cells (see Fig. 2).

A summary of the obtained electromagnetic calibration constants for the TileCal modules is presented in [4, 5, 6]. This information can be used to study of the transition effect. This effect manifests itself in the difference between the electromagnetic and *mip* (minimum ionizing particle) responses ($e/mip < 1$).

The aim of this work is a study of the transition effect, its behaviour as a function of the absorber thickness and its description by the GEANT4 (version 6.2) Monte-Carlo simulation.

These results will be important for the understanding of the TileCal electromagnetic energy scale.

2 Test beam setup

The TileCal calibration program with electrons, pions and muons was performed in the H8 beam at the CERN SPS. The test beam setup, shown in Fig. 1, is the following. The Barrel Module 0 is the bottom module mounted on the table. The middle layer is the production barrel module BM±. The top layer consists of the two extended barrel modules: EBM+ for $\eta > 0$ (beam left) and EBM− for $\eta < 0$ (beam right).

The layout of the readout cell geometry for modules is shown in Fig. 2. Each cell is a set of scintillating tiles connected by fibers to 2 PMTs. An innovative feature of this calorimeter is the orientation of the scintillators

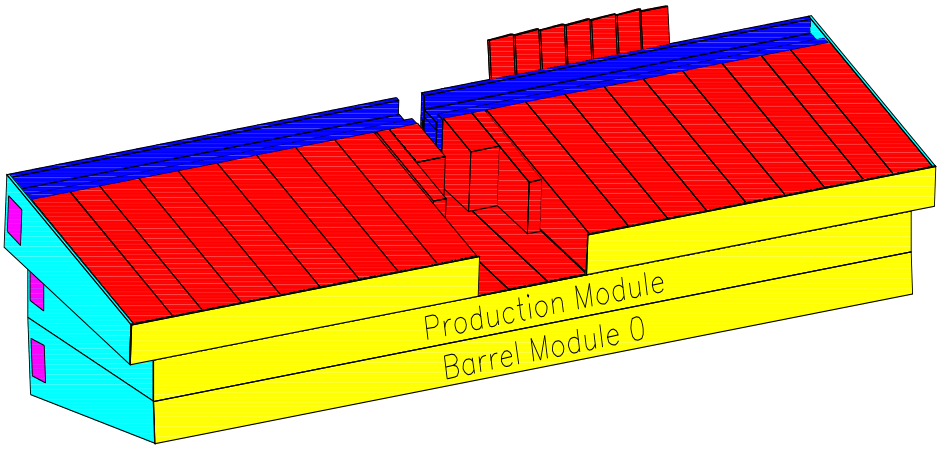

Figure 1: Sketch of the TileCal test beam setup.

that are placed in planes perpendicular to the colliding beams (Fig. 3, left).

Each module is read out in three longitudinal layers. The first layer consists of A cells, the second one of B and C cells, and the third one of D cells. There are 11 transverse rows of tiles (tilerows) in a module. The A cells for a barrel module have tilerows from 1 to 3, B and C cells — from 4 to 7, D cells — from 10 to 11. The A cells for an extended barrel module have tilerows from 1 to 3, B and C cells — from 4 to 6, D cells — from 7 to 11.

The iron structure of each module consists of a number of repeated periods (Fig. 3, right). Each period is 18 mm thick and consists of four layers. The first and third layers are formed by large trapezoidal steel plates (master plates), and spanning the full longitudinal dimension of the module. In the second and fourth layers, smaller trapezoidal steel plates (spacer plates) and scintillator tiles alternate. These layers consist of 11 different trapezoids of steel and scintillator, each spanning from 97 to 187 mm. The master plates, spacer plates and scintillator tiles are of 5 mm, 4 mm and 3 mm thick, respectively. The iron to scintillator ratio is $4.67 : 1$ by volume.

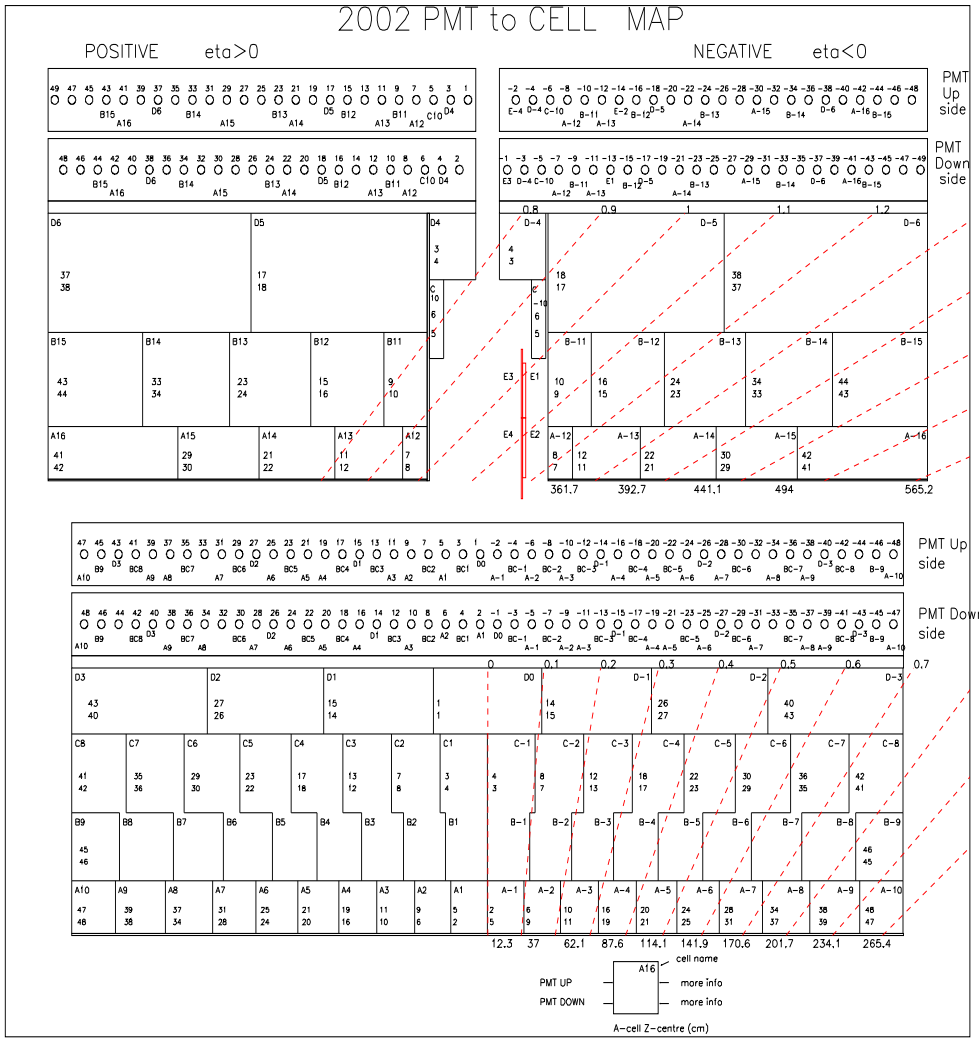

Figure 2: Layout of the TileCal modules cell geometry: for the extended barrel (top) and barrel (bottom) modules.

3 Sampling fraction of TileCal

The ATLAS Tile hadronic calorimeter belongs to the class of sampling calorimeters. An important parameter characterizing such calorimeters is the sampling fraction, SF, which is defined as a ratio of the energy deposited by minimum ionizing particles (*mip*) in the active, readout calorimeter layers to the total energy deposited by such particles in the

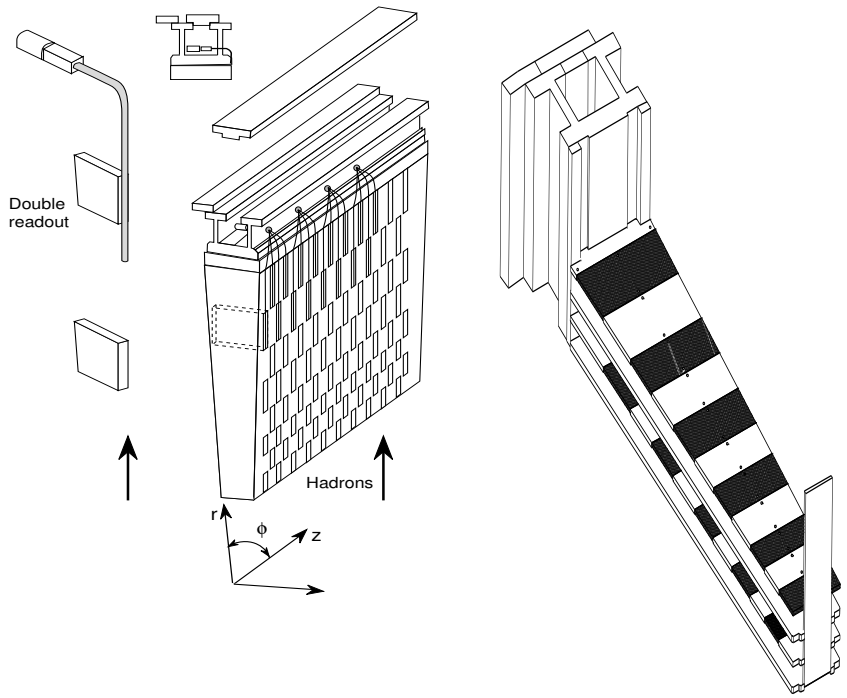

Figure 3: Sketch of the TileCal module (left). Exploded view of an assembled TileCal period (right).

calorimeter [7].

The sampling fraction of the TileCal is

$$SF_{mip} = \frac{\left(\frac{dE}{dx}\right)_{Sc} \cdot s}{\left(\frac{dE}{dx}\right)_{Sc} \cdot s + \left(\frac{dE}{dx}\right)_{Fe} \cdot t + \left(\frac{dE}{dx}\right)_{Glue} \cdot u} \ , \qquad (1)$$

where $(dE/dx)_{Sc} = 1.99$ MeV/cm, $(dE/dx)_{Fe} = 11.42$ MeV/cm and $(dE/dx)_{Glue} = 1.745$ MeV/cm [8] are the *mip* ionizing energy losses per unit length, $s = 0.3$ cm, $t = 1.405$ cm and $u = 0.1$ cm [3] are, respectively, the thicknesses of the readout (Sc), absorber (Fe) layers and glue (Glue) between absorber layers.

So, the quantity SF_{mip} for the TileCal is equal to 3.56 %.

While this definition of the sampling fraction (see formula (1)) is extremely simple and straightforward, there is not direct connection of calculated SF_{mip} with the TileCal experimental data.

4 The transition effect

The signal from an initial electron absorbed in a sampling calorimeter is the result of the ionization or excitation of the active calorimeter layers by all shower electrons and positrons that traverse these layers. Naively, one might therefore expect this signal to be equal to the signal from *mip*s that traverse the detector structure and whose combined energy deposit is equal to the initial energy of the showering electron ($e/mip = 1$).

Experimental data, independently obtained with a large number of different calorimeters, show that: in sampling calorimeters where the Z value of the absorber material is larger than the (average) Z value of the active medium, the response to electromagnetic showers is smaller than the response to *mip*s ($e/mip < 1$). The larger this difference is in Z, then the smaller the value of e/mip becomes. In calorimeters using high-Z absorber materials, such as lead or depleted uranium, e/mip values as low as 0.6 have been measured [9, 10, 11, 12].

The suppression of the electromagnetic shower response in sampling calorimeters with high-Z absorber material became historically known under the name **transition effect**. This term was introduced by Pinkau [13] who assumed that the phenomena should be attributed to mechanisms affecting the shower composition at the boundary between layers of materials with different Z. But this is not true.

Full understanding of the e/mip ratio behavior came later [7, 14]. Electromagnetic showers consist of two rather well-separable components: the hard part (> 1 MeV) that can be reasonably described as a bunch of *mip*s and the soft part (< 1 MeV) [15]. It turned out that the e/mip ratio value of calorimeters is crucially affected by phenomena that take place at energies corresponding to $< 10^{-4}$ of the energy of an incident particle.

When an electromagnetic shower develops, a large fraction of the initial electron energy is used to produce large numbers of low-energy (< 1 MeV) bremsstrahlung photons. These soft γ's dominate at the tails of the showers and are absorbed by four different processes (the photoelectric effect, coherent (Rayleigh) scattering, incoherent (Compton) scattering and electron-positron pair production) overwhelmingly in the absorber layers. The dominating process of the γ absorption in this energy range for iron is the Compton scattering [7].

As a result the soft electrons are produced: from EGS4 simulation, in

the case of iron, 34 % of the shower energy is deposited by electrons softer than 1 MeV [7] for a beam energy of 10 GeV. Their range is very short (about 1 mm for 1 MeV electron in iron [7]). Thus, these electrons only contribute to the calorimeter signal if the interactions occur in a very thin region, with an effective thickness δ, near the boundary between the active and passive layers. The *e/mip* ratio depends on the thickness of the absorber layers and also on the thickness of the active layers [15]. If the sampling frequency (the number of active layers per radiation length of material) is increased, i.e. if the absorber layers are made thinner, then δ represents a larger fraction of the total absorber volume. Therefore, a fraction of the shower γs that interact in the δ region increases and so does the response for electromagnetic showers.

5 Experimental determination of e/mip

The experimental determination of the *e/mip* ratio is a non-trivial issue [7]. It is necessary to measure the electron and *mip* responses. However, the response to *mip*s cannot be measured directly, because a *mip* is an unreal, imaginary particle. As soon as a real charged particle with an energy E for which dE/dx reaches its minimum value starts travelling through matter, it loses energy and therefore ceases to be a *mip*. The closest thing to a *mip* that in nature provides us is a muon. However, even muons with an energy as low as 5 GeV are by no means *mip*s. Since they are extremely relativistic ($\gamma = E/m_\mu \simeq 50$), their energy loss per unit length (14.5 MeV/cm in iron) is noticeable larger than the minimum ionizing value (11.4 MeV/cm in iron) [16].

The increased specific ionization of muons with energies larger than the minimum ionizing value is due to phenomena such as δ-ray emission (relativistic rise), bremsstrahlung, e^+e^- pair production and, at very high energies, nuclear reactions. The contribution of these effects to the total energy loss is strongly dependent on the muon energy and on (the Z value of) the traversed material. In practice, the experimental calorimeter response to *mip*s is determined from the signal distributions measured for muons of different energies, by estimating the consequences of the above effects, thereby unfolding the *mip* part of the calorimeter signals [10, 11, 12], [17].

In [17] the *e/mip* ratio has been determined for the TileCal prototype

modules at $\theta = 10^o$. The following expression has been used:

$$\frac{e}{mip} = \frac{R_e}{\left(\frac{Q_\mu}{E^{Cal}_{mip}}\right) \cdot \left(\frac{E^{Sc}_{mip}}{E^{Sc}_{\mu,\ MC}}\right)} \ , \tag{2}$$

where $R_e = \frac{Q_e}{E_{beam}}$ (pC/GeV) is the normalised electron response, Q_e (Q_μ) is the electron (muon) response (charge, pC), E^{Cal}_{mip} (GeV) is the *mip* energy loss in the calorimeter, E^{Sc}_{mip} (GeV) is the *mip* energy loss in the scintillators of the calorimeter, $E^{Sc}_{\mu,\ MC}$ (GeV) is the Monte-Carlo simulated muon energy loss in the scintillators of the calorimeter. The ratio $E^{Sc}_{mip}/E^{Sc}_{\mu,\ MC}$ plays the role of correction to difference of *mip* from muon. The denominator in (2) may be considered as a *mip* in units pC/GeV.

Since the structure of the Tile calorimeter prototype (Prot) and the production modules (Mod) is the same on what concerns the thicknesses of the iron and scintillators and their orientation the corresponding *e/mip* values should be equal for these modules. So, for $\theta = 10^o$

$$\left(\frac{e}{mip}\right)_{Mod,\ 10^o} = \left(\frac{e}{mip}\right)_{Prot,\ 10^o} . \tag{3}$$

Therefore, the value of *e/mip* at $\theta = 10^o$ for prototype modules and the electron responses of production modules obtained in this work was used for the determination of the *e/mip* values for production modules at other angles as follows:

$$\left(\frac{e}{mip}\right)_\theta = \left(\frac{e}{mip}\right)_{Prot,\ 10^o} \cdot \frac{R_{e,\ \theta}}{R_{e,\ 10^o}} \ . \tag{4}$$

6 Results

6.1 Monte-Carlo calculations

We have performed Monte-Carlo calculations (open circles) by using the GEANT4 toolkit [18] under the ATHENA framework (ATLAS Release 9.2.0 [19], GEANT4 version 6.2, QGSP_GN 2.5 Physics List). The comparison of GEANT4 6.2 results with GEANT 5.2, 7.0 and 8.0 is discussed in the Appendix (see section 8).

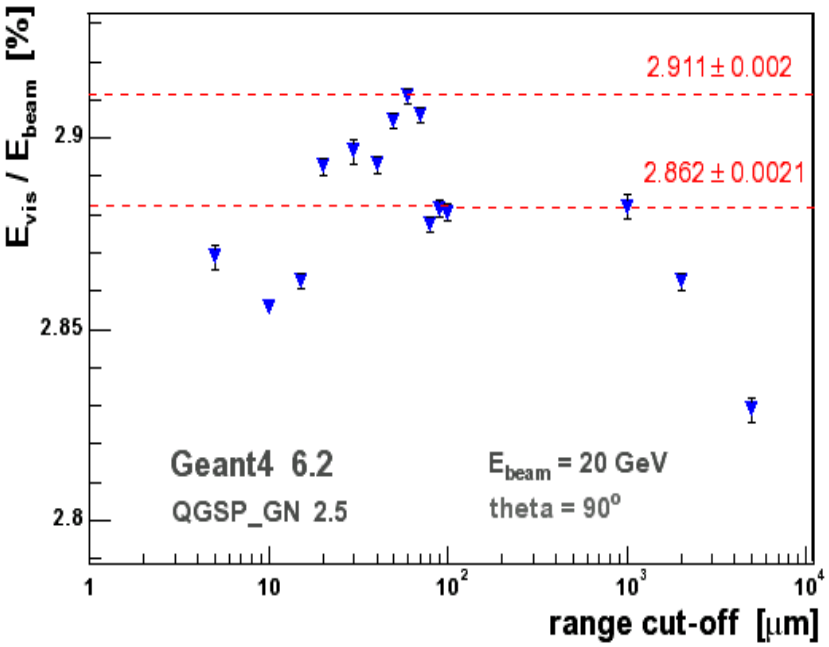

Figure 4: Normalized visible energy (E_{vis}/E_{beam}) deposition in scintillators as a function of the Range cut-off value for simulation of 20 GeV electrons at 90^o.

To accept maximal electron energy deposition in the active regions of the TileCal we investigated the optimal GEANT4 (version 6.2) Range cut-off value (see Fig. 4). For this study a setup of the Tile calorimeter modules was simulated so that — the electron beam was passing through endplate, spacer plate before entering in a scintillator tile. So, we had enhanced absorbtion conditions at the beginning of the electron shower development to reinforce an effect of Range cut-off dependence.

We got the maximum of the normalized visible energy (E_{vis}/E_{beam}) deposition in the active region of TileCal was found at a Range cut-off of equal to 60 μm. The difference between values of visible energies at this Range cut-off and for the mostly used Range cut-off in ATLAS (equal to 1 mm) is 1.7 %.

For *e/mip* Monte-Carlo calculations we chosen several angles (at 70, 80, 90 degrees) to scan Tile calorimeter modules from a back plate side by electron beams (36 mm in width).

In order to agree the test beam setup at 90^o we have chosen two different TileCal Monte-Carlo setups. The first setup was described above, the other Monte-Carlo setup of the Tile calorimeter modules that was used considers that the electron beam was passing through the endplate then a scintillator tile, spacer and master plates (see the dotted line of detailed scintillator tile on the Fig. 3, left). In this second case for the Range cut-off of equal to 60 μm the electron sampling fraction of the Tile calorimeter is (2.944 ± 0.002) %. For comparison with experimental data we have used the average value of electron response at 70, 80 and 90 degrees for both Monte-Carlo setups.

In the Table 1 we present the final Monte-Carlo result for 20 GeV electrons at 90^o: normalized visible energy, calorimeter sampling fraction (see section 3) and *e/mip* ratio for optimal range cut-off for electrons. The average Monte-Carlo calculated electron sampling fraction equal to (2.928±0.002) % is in good agrement with sampling fraction (2.9±0.1) % obtained in [17].

Table 1: The Monte-Carlo calculation of normalized visible energy (E_{vis}/E_{beam}), calorimeter sampling fraction (*mip*) and *e/mip* ratio for optimal range cut-off for electrons. These values are calculated at 90^o for two setups, e.g. when electrons enter first on an absorber or on a scintillating tile.

Range cut-off (mm)	Type of setup	E_{vis}/E_{beam} (%)	SF_{mip} (%)	*e/mip*
0.06	absorber/tile	2.911±0.002	3.567	0.816±0.005
	tile/absorber	2.944±0.002	3.567	0.825±0.005
	Average	2.928±0.002	3.567	0.821±0.004

A scan from front plate side was done for the angles at 3, 10, 20 and 30 degrees. Electron beams were shooting at the same area, 36 mm in width, of the middle module.

The Fig. 5 shows a dependence of Monte-Carlo calculated *e/mip* values for the TileCal for the 20 GeV electrons as a function of the incident Θ angle. The simulated an d experimental *e/mip* values are well described

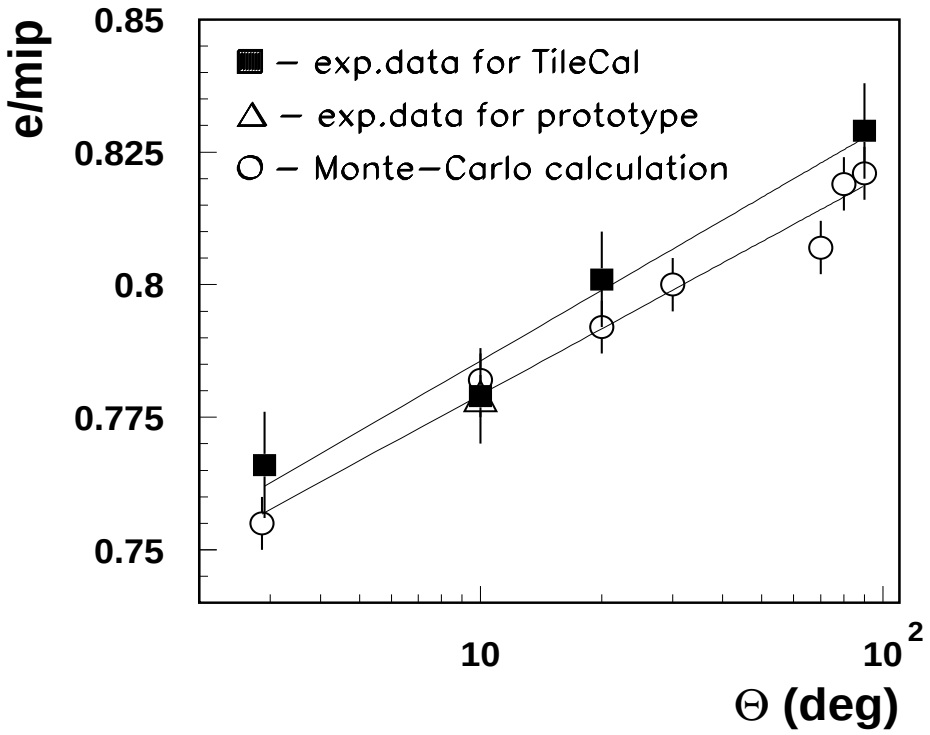

Figure 5: Monte-Carlo calculations (GEANT4 version 6.2) of the *e/mip* ratio for the TileCal test beam setup as a function of the impact angle of 20 GeV electrons (open circles). The experimental points are for TileCal production modules (black squares) and for TileCal prototype (open triangle) will be described in section 6.2. The curve is the result of the fit Monte-Carlo and experimental results by the formulae (5) and (6), respectively.

by the formulae, respectively,

$$\left(\frac{e}{mip}\right)_{mc} = (0.738 \pm 0.006) + (0.018 \pm 0.002) \cdot \log(\Theta) \ , \qquad (5)$$

$$\left(\frac{e}{mip}\right)_{exp} = (0.735 \pm 0.011) + (0.020 \pm 0.004) \cdot \log(\Theta) \ . \qquad (6)$$

As it can be seen, when the angle increases the *e/mip* ratio logarithmi-

cally increases. The difference between the *e/mip* values at 20^o and 90^o is 4.1 %.

6.2 Experimental results

To normalize our experimental data we have used the value of *e/mip* ratio of equal to 0.779±0.004 which is the weighted average of the *e/mip* (mean) values at different energies (10 – 300 GeV) given in the Table 3 (column "*e/mip* mean") obtained in [17] for $\theta = 10^o$ with $t_{abs} = 4.6\ X_0$ (a triangle in Fig. 6).

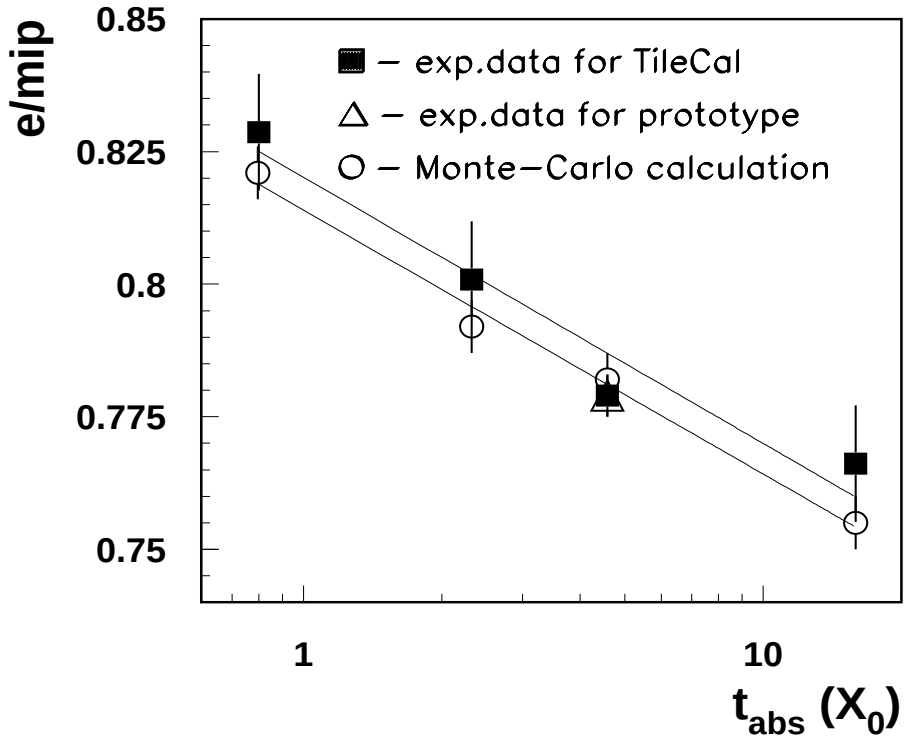

Figure 6: The *e/mip* ratio as a function of the absorber thickness (in radiation lengths). Experimental points are black squares. The open triangle is the prototype result published in [17]. The GEANT4 (version 6.2) Monte-Carlo calculations for the TileCal test beam setup are indicated in open circles. The curve is the result of the fit experimental and Monte-Carlo results by the formulae (7) and (8), respectively.

The *e/mip* values for angles 3, 20 and 90 degrees have been determined using the electromagnetic energy calibration constants $R_{e,\theta}$ (for

angles 3, 10, 20, 90 degrees) obtained in [5, 6] in the equation (4).

Results are shown in Fig. 6 as a function of the absorber thickness (in radiation lengths, X_0) at $t_{abs} = 0.8X_0$ ($\theta = 90^o$), $2.3X_0$ ($\theta = 20^o$), 4.6 X_0 ($\theta = 10^o$) and $15.9X_0$ ($\theta = 3^o$) (black squares).

The experimental and Monte-Carlo *e/mip* values are well described by the formulae, respectively,

$$\left(\frac{e}{mip}\right)_{exp} = (0.820 \pm 0.007) - (0.022 \pm 0.004) \cdot \log\left(t_{abs}\right) , \qquad (7)$$

$$\left(\frac{e}{mip}\right)_{mc} = (0.814 \pm 0.004) - (0.022 \pm 0.002) \cdot \log\left(t_{abs}\right) . \qquad (8)$$

As it can be seen, when the absorber thickness increases the *e/mip* ratio decreases logarithmically with X_0.

We have compared the experimental values of the *e/mip* ratio with these GEANT4 (version 6.2) Monte-Carlo calculations in the Fig. 6. The agreement is observed.

So, we experimentally observed the transition effect (*e/mip* < 1) and, for the first time, we discovered its behaviour as a function of the absorber thickness. The GEANT4 (version 6.2) Monte Carlo simulation results are in good agreement with the experimental data.

7 Conclusions

With the aim of establishing the electromagnetic response energy scale of the ATLAS Tile calorimeter and understanding the performance of the calorimeter to electrons 12 % of the modules have been exposed to electron beams with various energies.

On the basis of the obtained electromagnetic calibration constants we have determined the *e/mip* values in function of the absorber thickness using different beam incident angles.

We have observed the transition effect (*e/mip* < 1) and, for the first time, its behaviour as a function of the absorber thickness — the *e/mip* ratio decreases logarithmically when the absorber thickness increases and this is well described by the GEANT4 (version 6.2) Monte-Carlo simulation.

These results are important for precision electromagnetic energy scale determination for the ATLAS Tile calorimeter.

8 Appendix

Fig. 7 shows a dependence of Monte-Carlo GEANT4 (version 6.2) calculated normalized visible energy E_{vis}/E_{beam} values for the ATLAS HEC calorimeter for 100 GeV electrons and for the ATLAS Tile calorimeter for 20 GeV electrons as a function of the Range cut-off value. The

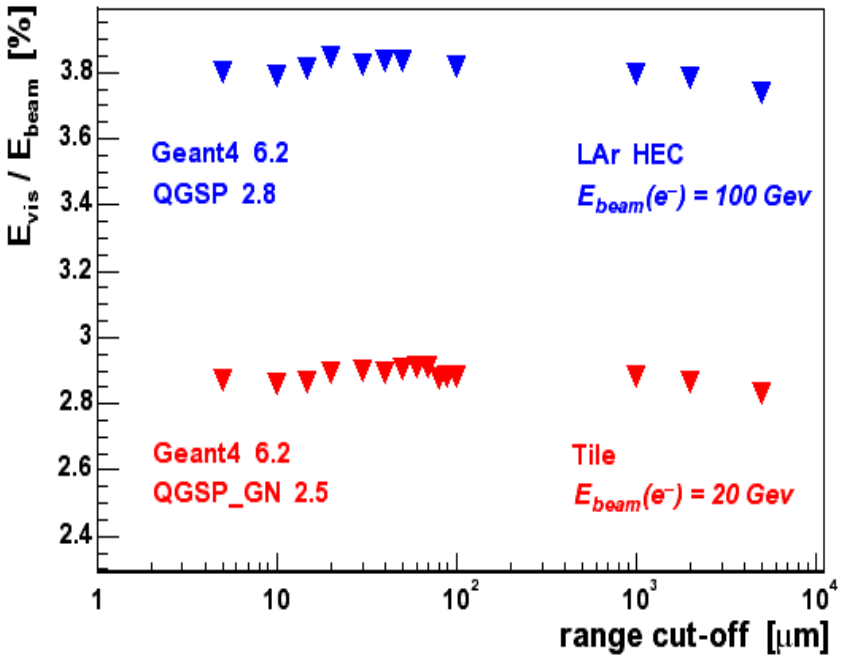

Figure 7: Normalized visible energy (E_{vis}/E_{beam}) deposition in LAr gap for ATLAS HEC calorimeter (top) for 100 GeV simulation electrons and in scintillators for ATLAS Tile calorimeter (bottom) as a function of the Range cut-off value for 20 GeV simulation electrons at 90^o.

shapes for the both distributions are very similar but E_{vis}/E_{beam} is 35 % larger for the ATLAS HEC calorimeter. The best Range cut-off for HEC calorimeter and Tile calorimeter is a bit different: 20 μm and 60 μm, respectively.

In the study [20] with GEANT4 version 8.0 of 100 GeV electrons response in the ATLAS HEC calorimeter was observed that maximal visible energy of electromagnetic showers is 2.5 % higher than in GEANT4 versions 5.2, 6.2 and 7.0 simulations and the experimental result. At the

same time the GEANT4 versions 5.2, 6.2 and 7.0 simulations results for maximal visible energy at HEC Range cut-off equal to 20 μm are in good agreement with the experimental result [20].

9 Acknowledgements

This work is the result of the efforts of many people from the ATLAS TileCal Collaboration.

The authors are greatly indebted to all Collaboration for test beam setup and data taking. The authors are thankful to T. Davidek, A. Kiryunin, I. Vichou and G. Usai for valuable discussions. We are very thankful to J. Maneira and L. Nodulman for precise correcting and kind suggestion. The authors are also very thankful to many other colleagues who are taking part in ATLAS TileCal test beam experiments.

The presented work was partly supported by INTAS-CERN grant number 03-52-6477.

References

[1] ATLAS Collaboration, ATLAS Technical Proposal, CERN/LHCC/ 94-43, 1994, CERN.

[2] ATLAS Collaboration, ATLAS Detector and Physics Performance, Technical Design Report, ATLAS TDR 15, CERN/LHCC/ 99-15.

[3] ATLAS Collaboration, ATLAS Tile Calorimeter Technical Design Report, CERN/LHCC/96-42, 1994, CERN.

[4] Y.A.Kulchitsky, V.B.Vinogradov, Performances of the ATLAS Hadronic Tile Calorimeter modules for Electrons and Pions, ATL-TileCal-2004-013, CERN.

[5] J.A. Budagov, J.I. Khubua, Y.A. Kulchitsky, N.A. Rusakovitch, P.V. Tsiareshka, V.B. Vinogradov, Electromagnetic Energy Calibration of the TileCal modules with the Flat Filter Method (July 2002 Test Beam Data), ATL-TileCal-PUB-2005-003, CERN, Geneva, Switzerland.

[6] Y.A.Kulchitsky et al, Summary of the Electromagnetic Calibration Constants at 20^o and 90^o for the TileCal modules, to be published as ATLAS note, CERN.

[7] R. Wigmans, Calorimetry, Energy Measurement in Particle Physics, Oxford University Press, Oxford, 2000.

[8] Particle Data Group, Phys. Letters **B592** (2004) 1.

[9] A. Andresen et al., NIM **A290** (1990) 95.

[10] T. Akesson et al., NIM **A262** (1987) 243.

[11] E. Bernardi et al., NIM **A262** (1987) 229.

[12] D. Acosta et al., NIM **A320** (1992) 128.

[13] K. Pinkau, Phys.Rev. **B139** (1965) 1548.

[14] J. del Peso, E. Ros, NIM **A295** (1990) 330.

[15] R. Wigmans, NIM **A265** (1988) 273.

[16] W. Lohmann et al., CERN 85-03.

[17] Z. Ajaltouni, et al., NIM **A388** (1997) 64; Preprint CERN: CERN-PPE-96-173, Geneva, CERN, 1996.

[18] S. Agostinelli, et al., Response of the ATLAS Tile Calorimeter prototype to muons; NIM **A506** (2003) 250.

[19] http://atlas.web.cern.ch/ATLAS/GROUPS/SOFTWARE/OO/dist/

[20] A. Kiryunin, Status of MC validation with HEC testbeam data, web page: http://cds.mppmu.mpg.de/cdsagenda/fullAgenda.php?ida=a064, ATLAS Hadronic Calibration Workshop, 4 May, Munich; and web page: http://agenda.cern.ch/fullAgenda.php?ida=a062331, LCG Physics Validation for LHC Simulations meeting, 10 May, CERN.